The Optimal Paper Moebius Band and Finite Tensegrity Calculations

Richard Evan Schwartz *

November 5, 2020

Abstract

There are two main conjectures about paper Moebius bands. First, a smooth embedded paper Moebius band must have aspect ratio at least $\sqrt{3}$. Second, any sequence of smooth embedded paper Moebius bands having aspect ratio converging to $\sqrt{3}$ converges, in the Hausdorff topology and up to isometries, to an equilateral triangle of semi-perimeter $\sqrt{3}$. We will reduce these conjectures to a finite number of statements about the positivity of certain piecewise algebraic expressions. The reader should view this document as a set of research notes rather than as a finished paper.

1 Introduction

A *paper Moebius band* of aspect ratio λ is a smooth isometric embedding $I : M_\lambda \to \boldsymbol{R}^3$, where M_λ is the flat Mobius band

$$M_\lambda = ([0,1] \times [0,\lambda])/\sim, \qquad (x,0) \sim (1-x,\lambda) \tag{1}$$

An early work [**Sa**] establishes the existence of paper Mobius bands. The main question about these objects is the value of the smallest λ_0 such that a paper Moebius band of aspect ratio λ exists iff $\lambda > \lambda_0$. B. Halpern and C. Weaver [**HW**] show that $\lambda_0 \in [\pi/2, \sqrt{3}]$. The book [**FT**, §14] gives an excellent exposition of these bounds. The paper [**CF**] gives a general framework

*Supported by N.S.F. Grant DMS-1807320

for understanding objects like smooth paper Moebius bands. See [**AHLM**], [**CKS**], [**HF**], [**MK**], [**GS**] for work that is more or less related.

Halpern and Weaver make the following conjecture about λ_0.

Conjecture 1.1 (Optimality) *A smooth embedded paper Moebius band has aspect ratio greater than* $\sqrt{3}$*. Hence* $\lambda_0 = \sqrt{3}$*.*

The upper bound $\lambda_0 \leq \sqrt{3}$ is explained by an example. Figure 1.1 shows an immersed polygonal paper Mobius band of aspect ratio exactly $\sqrt{3}$.

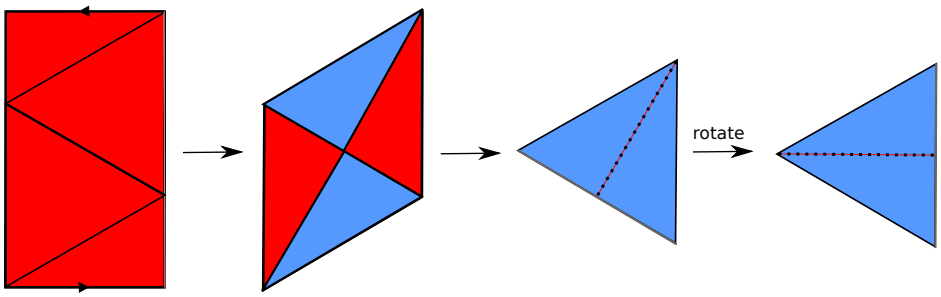

Figure 1.1: The conjectured optimizer

The final image is not embedded. It is an equilateral triangle of semi-perimeter $\sqrt{3}$. However, for any $\epsilon > 0$, one can approximate this map by smooth embeddings of $M_{\lambda+\epsilon}$. See [**FT**] for a discussion about this.

Here is an elaboration on the Optimality Conjecture:

Conjecture 1.2 (Rigidity) *A sequence of smooth embedded paper Mobius bands having aspect ratio converging to* $\sqrt{3}$ *converges, in the Hausdorff metric and up to isometries, to an equilateral triangle of semi-perimeter* $\sqrt{3}$*.*

In [**S2**] we show that $\lambda_0 > \sqrt{3} - (1/26)$. The actual bound involves a complicated algebraic number that is just slightly larger than this. For comparison, $\pi/2 < \sqrt{3} - (4/26)$, so our bound gets more than 3/4 of the way to the conjectured optimal bound. We also proved a result [1] which contains Theorem 3.1 as a subset.

In [**FT**] it is pointed out that (probably) the main difficulty in proving the conjectures is figuring out how to use the topological hypothesis that the paper Moebius band is embedded. Indeed, in [**FT**], the authors give an

[1]The result in Theorem 3.1 has a constant $\sqrt{3} - (1/24)$, which differs slightly from the bound $\sqrt{3} - (1/26)$. This is not a typo. The new constant refers to different objects.

example of a sequence of immersed examples with aspect ratio converging to $\pi/2$. So, something more is needed. In this paper, which is a sequel to [**S2**], we will reduce the Optimality and Rigidity Conjectures to a finite number of purely geometric estimates.

All but four of the geometric estimates seem true by a fairly wide margin. They reduce to statements that certain explicit piecewise algebraic expressions are positive on either $[0,1]^{10}$ or $[0,1]^{14}$. These estimates all feed into our main topological result, which we call the Topology Lemma. The remaining four geometric estimates feed into a result which I call the Geometry Lemma. These are more delicate because the case of the presumed optimizer is a boundary case.

Here is the extent to which I have experimented with these calculations:

- I have experimented extensively with the calculations which go into the Topology Lemma, and I will detail these experiments in §7. These all seem to work by wide margins.

- I have experimented extensively with the two calculations which mirror Cases 1 and 2 of the Geometry Lemma. These seem to work out.

- A third calculation, which would have finished Cases 3 and 4 of the Geometry Lemma simultaneously, did not work. I replaced this one calculation with two separate calculations, each of which more tightly mirrors the corresponding case of the Geometry Lemma. I have not yet experimented with these.

The estimates are all closely related to tensegrities. A *tensegrity* is essentially a graph graph labeled with positive numbers. Some of the edges are considered to be rigid, like metal rods, and some of the edges are considered to be flexible, like pieces of rope. An embedding of the tensegrity is a map from the graph into space so that the length of each wooden edge is exactly equal to the label and the length of each rope edge is at most the label. See [**CB**] for a survey.

A paper Moebius bend behaves somewhat like a tensegrity. It is ruled by a continuous family of line segments which, individually, are completely rigid. These are like the wooden edges. The directions transverse to the bend lines are like the rope edges; they are drawn together by the spatial embedding. By remembering just a finite number of bends, we can approximate a paper Moebius band by a finite tensegrity. The advantage is that we replace an

infinite dimensional space by essentially a projection onto a finite dimensional space. The disadvantage is that we might be forgetting vital information.

Here is an overview of the paper. I have tried to structure the paper so that you only have a read about 5 more pages before you see the overall structure of the proof.

In §2 I prove the Optimality Theorem and the Rigidity Theorem modulo two main results, the Geometry Lemma and the Topology Lemma. The Geometry Lemma also works in the immersed case (with a side condition concerning something called a T-pattern) and the Topology Lemma requires an embedding. The rest of the paper is devoted to reducing these two results to geometric estimates, most of which are handled by tensegrity calculations.

In §3 I recall some geometric estimates from [**S2**] and also prove a new one along similar lines. The precise constants in these results are not important. They mainly serve to give us some *a priori* bounds which help us set up the limits and targets of our calculations.

In §4 I introduce the tensegrities which are used in the calculations.

In §5 I reduce the Topology Lemma to tensegrity calculations. The Topology Lemma is a very natural statement which ought to have a traditional proof, but I don't know one.

In §6 I will reduce the Geometry Lemma to tensegrity calculations.

In §7 I will explain the extent to which I have experimented with the calculations.

I have posted my computer code on my website:
http://www.math.brown.edu/∼res/Java/MOEBIUS.tar

I would like to thank Dan Cristofaro-Gardiner, Dmitry Fuchs, Steve Miller, and Sergei Tabachnikov for helpful discussions about this problem. I would especially like to thank Sergei for telling me about the problem and pointing me to his book with Dmitry. I would also like to acknowledge the support of the Simons Foundation, in the form of a 2020-21 Simons Sabbatical Fellowship, and also the support of the Institute for Advanced Study, in the form of a 2020-21 membership funded by a grant from the Ambrose Monell Foundation.

2 The Proof modulo Two Lemmas

In this chapter we recall some concepts and results from [**S2**] and then reduce the two main theorems to two auxiliary lemmas, the Geometry Lemma and the Topology Lemma.

2.1 Polygonal Moebius Bands

Here are some detinitions taken from [**S2**].

Basic Definition: Say that a *polygonal Moebius band* is a pair $\mathcal{M} = (\lambda, I)$ where $I : M_\lambda \to \boldsymbol{R}^3$ is an isometric embedding that is affine on each triangle of a triangulation of M_λ. We insist that the vertices of these triangles all lie on ∂M_λ, as in Figure 1.1. Any smooth isometric embedding $I' : M_\lambda \to \boldsymbol{R}^3$ can be approximated arbitrarily closely by this kind of map, so it suffices to work entirely with polygonal Moebius bands.

Associated Objects: Let $\delta_1, ..., \delta_n$ be the successive triangles of $\mathcal{M}$.

- The *ridge* of δ_i is edge of δ_i that is contained in ∂M_λ.
- The *apex* of δ_i to be the vertex of δ_i opposite the ridge.
- A *bend* is a line segment of δ_i connecting the apex to a ridge point.
- A *bend image* is the image of a bend under I.
- A *facet* is the image of some δ_i under I.

We always represent M_λ as a parallelogram with top and bottom sides identified. We do this by cutting M_λ open at a bend. See Figures 1.1, 2.1, 3.1. In what follows, we will be more specific about which bend we choose to cut along.

T-Patterns: Say that a *T-pattern* is a pair of perpendicular coplanar disjoint bend images. figure 2.1 shows an example.

Now we explain one of the main results from [**S2**]. This result is the key to our whole approach. The bound of $7\pi/12$ in the next lemma is larger than $\sqrt{3}$, so we always have this bound for the examples of interest.

Lemma 2.1 *A polygonal Moebius band of aspect ratio less than $7\pi/12$ has a T-pattern.*

Sketch of the Proof: A pair of perpendicular bend images is contained in a pair of parallel planes. The small aspect ratio allows us to rotate the image so that the bend images all make an angle of less than $\pi/4$ with the XY-plane. This property guarantees that the parallel planes just mentioned never contain vertical line segments. We consider the space $\mathcal{P}$ of perpendicular pairs of bend images. Generically this space is a topological 1-manifold. We show that $\mathcal{P}$ contains a connected component $\mathcal{K}$ that is invariant under the involution which swaps the pair of bend images. Starting with a pair (α, β) of bend images in $\mathcal{K}$ we consider a path to (β, α). The corresponding pairs of perpendicular planes exchange their position and never contain vertical line segments. Hence, at some instant along the path, they coincide. ♠

Standard Normalization and Tame Pairs: The T-pattern in our polygonal Moebius band may not be unique, but we fix a T-pattern once and for all. Let β_1 and β_2 be two bends whose corresponding images $\beta_1^* = I(\beta_1)$ and $\beta_2^* = I(\beta_2)$ form a T-pattern. Since these segments do not intersect, we can label so that the line extending β_2^* does not intersect β_1^*. We cut M_λ open along β_1 and treat β_1 as the bottom edge. We now set $\beta_b = \beta_1$ and $\beta_t = \beta_2$ and (re)normalize as in §2.1. So, β_b^* connects $(-B, 0, 0)$ to $(0, 0, 0)$, and β_t^* is a translate of the segment connecting $(0, 0, 0)$ to $(0, T, 0)$. This translate still lies in the XY-plane. Here B and T are the lengths of these segments.

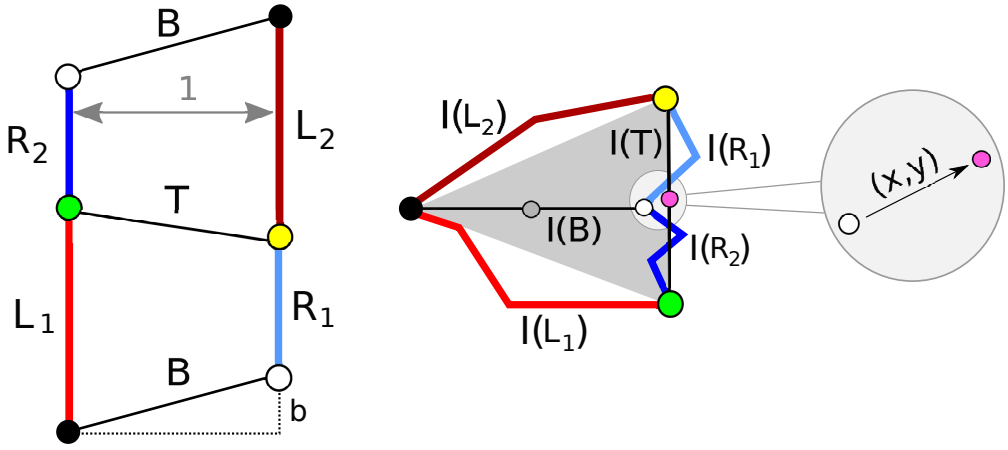

Figure 2.1: The standard normalization

The left side of Figure 2.1 shows M_λ. Reflecting in a vertical line, we normalize so that $L_1 \geq R_1$. This means that $L_2 \geq R_2$. We set

$$S_j = L_j + R_j. \tag{2}$$

We call this the *standard normalization*. We set $\lambda(\tau_1, \tau_2) = (S_1 + S_2)/2$ be the aspect ratio of the underlying polygonal Moebius band. We insist that $\lambda < \sqrt{3} + 10^{-100}$ and we call (τ_1, τ_2) a *tame pair*. We add this tiny constant because, for the Rigidity Theorem, we will need to consider examples having aspect ratio slightly larger than $\sqrt{3}$.

The right side of Figure 2.1 shows the T pattern, and the corresponding images of the sets on the left under the isometry I. The wiggly curves we have drawn do not necessarily lie in the XY-plane but their endpoints do. We normalize so that $(0, 0, 0)$ is the right endpoint of the B-bend image. In the figure (x, y) denotes the vector which points from the white to the pink vertex on the right side. We have blown this part of the figure up to make it more visible.

Remark: Actually, there are two such standard normalizations. We can make the replacements $M_\lambda \to \rho_1(M_\lambda)$ and $I \to \rho_2 \circ I \circ \rho_1$, where ρ_1 is reflection in the midpoint of M_λ and ρ_2 is reflection in the X-axis. This change preserves all our normalizations, and gives us the pair (τ_2, τ_1). Aside from swapping the names of the variables, the only thing that happens to Figure 2.1 is that the vector (x, y) changes to $(x, -y)$. This trick lets us interchange the roles of the indices in various arguments. So, if we prove a certain statement for (τ_1, τ_2) then we get the same result for (τ_2, τ_1).

2.2 Special Bends

We did a lot of numerical experiments and these led to the definitions we give here. Without these experiments, the definitions would seem very unmotivated.

Pitch: Given a polygonal Moebius band with a T-pattern, we use the standard normalization. For each bend β we let $\beta^* = \pi \circ I(\beta)$, the projection of the bend image $I(\beta)$ into the XY-plane. Each bend β of τ_1 has associated to it an angle $\theta \in [0, \pi]$ such that when we rotate the positive X-axis counterclockwise by θ we arrive at a ray parallel to β^*. We call θ the *bend pitch*.

Four Special Bends: Let $(k)_1$ stand for a bend β of τ_1 whose bend pitch is $+k\pi/12$. Let $(k)_2$ stand for a bend β of τ_2 whose bend pitch is $-k\pi/12$. We insist that $(0)_1 = (0)_2 = (0)$ is the bottom bend and $(6)_1 = (6)_2 = (6)$ is the top. We are interested in bends $(0), (1)_j, (4)_j, (6)$ for $j = 1, 2$. We pick $(1)_j$ and $(4)_j$ to be the bends nearest (0) and (6), respectively, which satisfy the conditions. Let π be projection into the XY-plane. We illustrate our notation with an example:

$$(4)_1^* = \pi \circ I((4)_1) \tag{3}$$

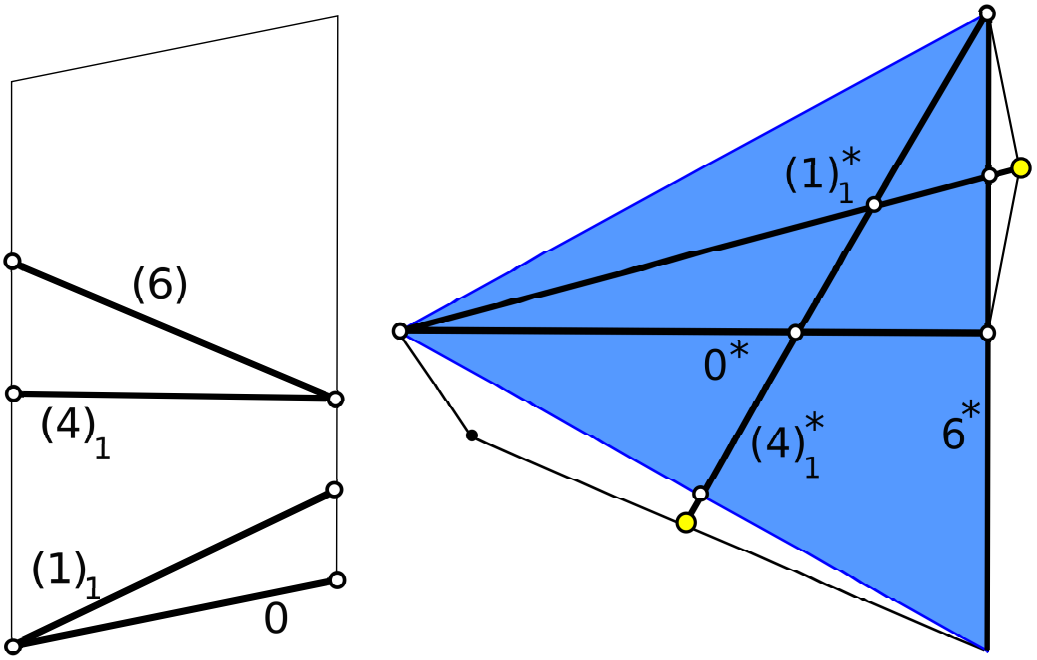

Figure 2.2: The 4 special bends and the yellow tips.

Tips and Bumps: We define the 1-*tip* of τ_j^* to be the right endpoint of $(1)_j^*$. We define the 4-tip of τ_j to be the left endpoint of $(4)_j^*$. These are the yellow vertices in Figure 2.2. Let Δ be the convex hull of the T-pattern. We say τ_j^* has a k-*bump* if the k-tip lies outside Δ. We make 2 more definitions:

- When $i \neq j$ we write $\tau_i \to_k \tau_j$ if some bend X of τ_i is such that X^* contains the k-tip of τ_j^*.
- We write $\tau_k \to_1 \tau_k$ if some bend $X \in [4, 6]_k$ is such that X^* contains the 1-tip of τ_k.

2.3 The Two Main Lemmas

Suppose we have a polygonal Mobius band of aspect ratio less than

$$\sqrt{3} + 10^{-100}.$$

In the first result we assume that $\mathcal{M}$ has a T pattern but we do not assume that $\mathcal{M}$ is embedded. In the second result we require that $\mathcal{M}$ is embedded.

In either case, $\mathcal{M}$ has a T patterm. Let (τ_1, τ_2) be the associated tame pair. For the sake of working with closed subsets of objects, we allow the limiting case when the horizontal and vertical segments $(0)^*$ and $(6)^*$ touch. That is, we allow $(0, 0, 0)$, the right endpoint of $(0)^*$, to lie in $(6)^*$.

Here is the main topological component of the proof. In this result we insist that $\mathcal{M}$ is embedded.

Lemma 2.2 (Topology) *Suppose that (τ_1, τ_2) is a tame pair corresponding to an embedded polygonal Moebius band. Then at least one of 4 things is true.*

$$\tau_1 \to_1 \tau_1, \qquad \tau_2 \to_1 \tau_1, \qquad \tau_1 \to_4 \tau_2, \qquad \tau_2 \to_4 \tau_1.$$

In the next result, which is purely geometrical, we do not assume that $\mathcal{M}$ is embedded. However, we do insist that $\mathcal{M}$ has a T-pattern, as above.

Lemma 2.3 (Geometry) *Suppose that (τ_1, τ_2) is a tame pair.*

1. *If $\tau_1 \to_1 \tau_1$ then $S_1 \geq \sqrt{3}$.*
2. *If $\tau_2 \to_4 \tau_1$ then $S_1 + S_2 \geq 2\sqrt{3}$.*
3. *If $\tau_1 \to_1 \tau_2$ and $\tau_2 \to_1 \tau_1$ then $S_1 + S_2 \geq 2\sqrt{3}$.*
4. *If $\tau_1 \to_1 \tau_2$ and $\tau_1 \to_1 \tau_1$ then $S_1 + S_2 \geq 2\sqrt{3}$.*

Moreover, for any $\epsilon > 0$ there is a $\delta > 0$ such that if we have equality within δ in any of the cases, then $(0)^* \cup (6)^*$ is within ϵ of an equilateral triangle of perimeter $2\sqrt{3}$ in the Hausdorff metric.

There is a symmetric result. Switching the roles of the indices, we get the same result when $\tau_2 \to_1 \tau_2$, etc. Thus, any of 8 hypotheses lead to the conclusion in the Geometry Lemma.

2.4 Proofs of the Main Results

Given an immersed polygonal Moebius band with a T-pattern, we get a tame pair (τ_1, τ_2) provided that the aspect ratio satisfies $\lambda < \sqrt{3} + 10^{-100}$. Most of this chapter is devoted to proving the following result.

Proof of the Optimality Theorem: If we have an embedded polygonal Moebius band of aspect ratio less than $\sqrt{3}$ then we cut it open along the bends corresponding to a T-pattern. This gives rise to a tame pair (τ_1, τ_2) with $S_1 + S_2 = \lambda(\tau_1, \tau_2) < 2\sqrt{3}$. We can order so that $S_2 < \sqrt{3}$. From the Geometry Lemma, it is impossible that $\tau_2 \to \tau_2$.

The Topology Lemma, applied to the pair (τ_2, τ_1), leaves 3 possibilities:

1. $\tau_1 \to_4 \tau_2$.
2. $\tau_2 \to_4 \tau_1$.
3. $\tau_1 \to_4 \tau_2$.

The Geometry Lemma rules out Cases 1 and 2.

Consider Case 3. Suppose $\tau_1 \to \tau_2$. Given the cases we have already ruled out, the the Topology Lemma applied to (τ_1, τ_2) tells us that, additionally, either $\tau_1 \to \tau_1$ or $\tau_2 \to \tau_1$. The Geometry Lemma now rules out these two cases. ♠

Proof of the Rigidity Theorem: Suppose we have a sequence of Paper Moebius bands whose aspect ratios converge to $\sqrt{3}$. The Topology Lemma applies for all examples sufficiently far along the sequence and thus we get a sequence $\{(\tau_{n,1}, \tau_{n,2}\})$ of tame pairs. By the Geometry Lemma, the convex hull Δ of the T pattern converges (modulo global isometries of $\boldsymbol{R}^3$) to the equilateral triangle Δ_0 of perimeter $2\sqrt{3}$. Since the length of the boundary $I(\partial M_\lambda)$ is at least as long as the perimeter of Δ, we see that this boundary must in fact converge in the Hausdorff Topology (modulo global isometries) to this same triangle Δ_0. This proves the Rigidity Theorem. ♠

3 A Priori Bounds

Theorem 3.1 and Lemma 3.2 are the main results in this chapter. The reader anxious to get to the main points should skip the proofs in this chapter and just use these results as black boxes. The precise statements of these results are not that important. We just need some *a priori* bounds to frame our calculations.

3.1 Geometric Bounds

Let Δ be the convex hull of the T-pattern $I(T) \cup I(B)$. Let b denote the slope of the B-bend and let t denote the slope of the T-bend. Figure 2.1 shows b but not t. Let Ω denote the set of pairs (b, t) which can arise in a standard pair with $\lambda < \sqrt{3}$. Figure 4.1 shows a plot of Ω in blue, as well as a quadrilateral $\widehat{\Omega}$ which we showed contains Ω.

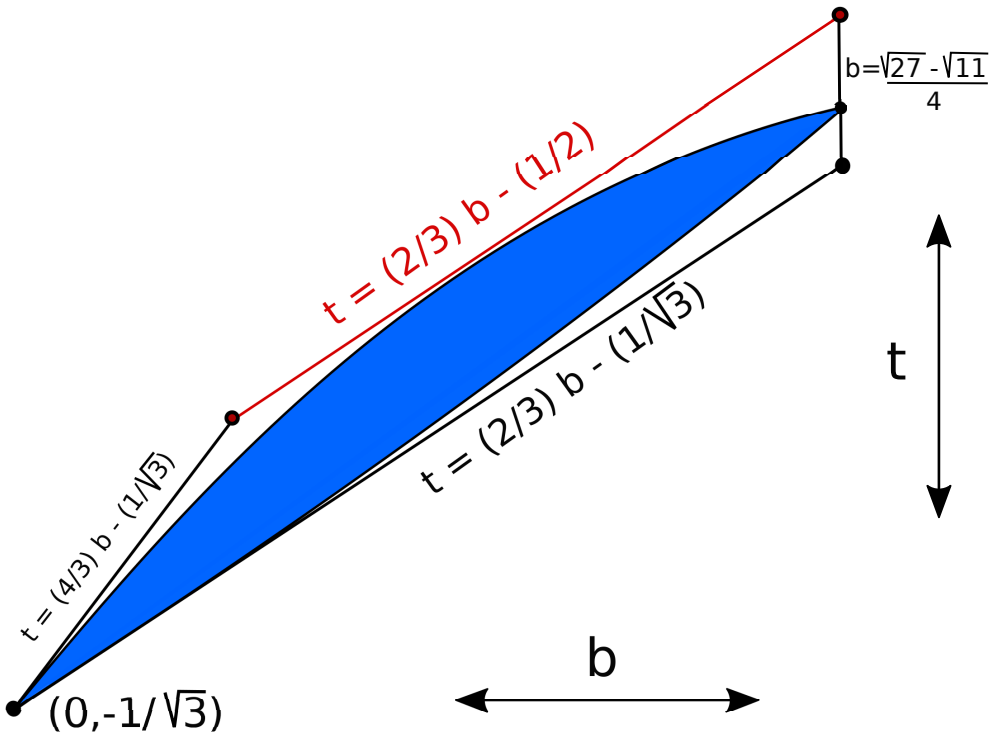

Figure 3.1: The range of slopes.

The following results are a subset of the main result in [**S2**, §4].

Theorem 3.1 *For any immersed paper Moebius with a T-pattern and aspect ratio less than $\sqrt{3}$, the following is true.*

1. $S_j \geq \sqrt{3} - (1/24)$ *for* $j = 1, 2$.
2. $x < 1/18$ *and* $|y| < 1/30$.
3. $\Omega \subset \widehat{\Omega}$.

Sketch of the Proof: The distances relations in Figure 2.1 give rise to 3 constraints:

1. $R_1 \geq \sqrt{x^2 + (T/2 - y)^2}$ and $R_2 \geq \sqrt{x^2 + (T/2 + y)^2}$.
2. $L_1 \geq \sqrt{(B + x)^2 + (T/2 + y)^2}$ and $L_2 \geq \sqrt{(B + x)^2 + (T/2 - y)^2}$.
3. $B^2 - L_j^2 + (T - R_j)^2 \leq 0$ for $j = 1, 2$.

Constraints 1 and 2 follow directly from the Pythagorean Theorem. Constraint 3 comes from a more subtle argument involving the Ridge Curve, which we define later in this chapter. We give the argument in [**S2**].

We also have the following relations:

$$L = \frac{S + b - t}{2}, \quad R = \frac{S - b + t}{2}, \quad B = \sqrt{1 + b^2}, \quad T = \sqrt{1 + t^2}. \tag{4}$$

Plugging these relations into our various constaints and doing some calculus, we arrive at the statements in Theorem 3.1. ♠

3.2 Angle Range Bounds

Now we prove a new result, similar in spirit to Theorem 3.1. This new result also helps frame our calculations by giving *a priori* bounds.

Let the interval $[0, 1]_1$ denote all the bends in the trapezoid τ_1 that interpolate between 0 and 1_1. Let $\Theta([0, 1]_1)$ denote the range of bend pitches for bend images in $[0, 1]_1$. (We make similar definitions for the other intervals.) The initial bend image $(0)^*$ has bend pitch 0. The final bend image $(1_1)^*$ has bend pitch $\pi/12$. It is tempting to guess that $\Theta([0, 1]_1) = [0, \pi/12]$ but, since the bend pitches need not vary monotonically, we cannot conclude this. In this section we establish the following bounds.

Lemma 3.2 *Let $\theta_0 = \pi/30$. For any tame pair (τ_1, τ_2) of trapezoids,*

1. $\Theta([0,1]_1) \subset [-\theta_0, \pi/12]$.
2. $\Theta([0,4]_1) \subset [-\theta_0, 4\pi/12 + \theta_0]$.
3. $\Theta([4,6]_1) \subset [4\pi/12, \pi/2 + \theta_0]$.

Remark: One consequence Lemma 3.2 is that any bend in τ_1 has pitch in $[-\theta_0, \pi/2 + \theta_0]$. This is a more precise version of the statement above that the pitches essentially lie in $[0, \pi/2]$ except for a bit of slope at either end.

The rest of the chapter is devoted to proving this result. The technique used here is not used anywhere else in this paper, though we used it extensively in [**S2**]. At this point, the reader can use Theorem 3.1 and Lemma 3.2 as black boxes. Again, they only serve to place *a priori* bounds on our tensegrity calculations.

3.3 The Ridge Curve

Here we recall some more notions from [**S2**].

The Sign Sequence: Let $\delta_1, ..., \delta_n$ be the triangles of the triangulation associated to $\mathcal{M}$, going from bottom to top in P_λ. We define $\mu_i = -1$ if δ_i has its ridge on the left edge of P_λ and $+1$ if the ridge is on the right. The sequence for the example in Figure 1.1 is $+1, -1, +1, -1$.

The Core Curve: There is a circle γ in M_λ which stays parallel to the boundary and exactly $1/2$ units away. In Equation 1, this circle is the image of $\{1/2\} \times [0, \lambda]$ under the quotient map. We call $I(\gamma)$ the *core curve*.

The left side of Figure 3.2 shows M_λ and the pattern of bends. The vertical white segment is the bottom half of γ. The right side of Figure 3.2 (which has been magnified to show it better) shows $I(\tau)$ where τ is the colored half of M_λ. All bend angles are π and the whole picture is planar. The colored curve on the right is the corresponding half of the core curve. Incidentally, for τ we have $L + R = 1.72121... < \sqrt{3}$.

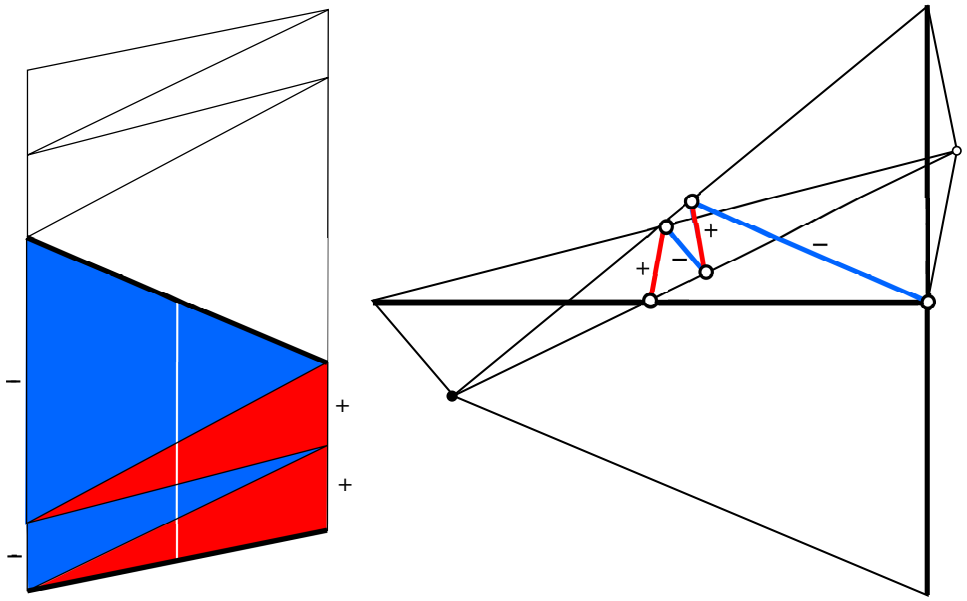

Figure 3.2: The bend pattern and the bottom half of the image

The Ridge Curve: We show the picture first, then explain.

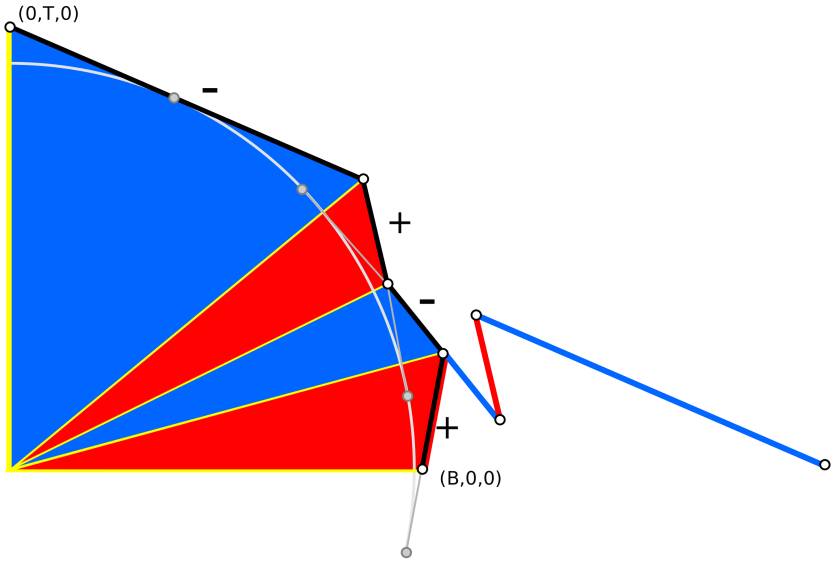

Figure 3.3: Half of the core curve (red/blue) and half of the ridge curve (black). The core curve is scaled up by a factor of 2.

Let β_b be the bottom edge of the parallelogram representing M_λ. We normalize so that I maps the right vertex of β_b to $(0,0,0)$ and the left vertex to $(-B,0,0)$, where B is the length of β_b. Let $E_1,...,E_n$ be the successive edges of the core curve, treated as vectors. Let

$$\Gamma_i' = 2\mu_i E_i, \qquad i = 1,...,n. \tag{5}$$

Let Γ be the curve whose initial vertex is $(B,0,0)$ and whose edges are $\Gamma_1',...,\Gamma_n'$. Here $\mu_1,...,\mu_n$ is the sign sequence.

Γ has length 2λ, connects $(B,0,0)$ to $(-B,0,0)$, and is disjoint from the open unit ball. The lines extending the sides of Γ are tangent to the unit sphere. We rotate so that Γ contains $(0,T,0)$ for some $T>1$. If we cone Γ to the origin, we get a collection $\Delta_1,...,\Delta_n$ of triangles, and Δ_i is the translate of $\mu_i I(\delta_i)$ whose apex is at the origin. In particular, the vectors pointing to the vertices of Γ are parallel to the corresponding bend images. Figure 3.3 shows the portion of the ridge curve (in black) associated to the example in Figure 2.1. We have also scaled the core curve by 2 and translated it to show the relationships between the two curves.

3.4 Proof of Lemma 3.2

Let us dispense with a representative case first. The reason why $\Theta([0,1]_1)$ ends at $\pi/12$ rather than $\pi/12+\theta$ for some positive θ is that we take $(1)_1$ be the first bend after $(0)_1$ with pitch $\pi/12$. Similar remarks apply to the other cases where we have no slop over the endpoint in the bound.

Now we consider the other cases. Let Γ_1 be the portion of the ridge curve associated to τ_1. The curve Γ_1 connects $(B,0,0)$ to $(0,T,0)$. This curve perhaps does not stay entirely in the positive sector consisting of points (x,y,z) with $x,y \geq 0$, but it certainly does not "go around the back". For instance, the projection $\pi(\Gamma_1)$ avoids the ray of slope 1 which starts at $(0,0)$ and goes through $(-1,-1)$. Here π is projection into the XY-plane.

Let Π_1 and Π_2 be two planes in $\boldsymbol{R}^2$ which contain the Z-axis. Suppose that the dihedral angle between Π_1 and Π_2 is θ. Suppose these planes are ordered so that Γ_1 must hit Π_1 before hitting Π_2. We give a lower bound on the length if Γ_1 goes from $(B,0,0)$ to a point $p \in \Pi_2$, to a point $q \in \Pi_1$ to $(0,T,0)$. Figure 3.4 shows what $\Pi(\Gamma_1)$ would look like in several cases.

It is worth pointing out that Γ_1 lies outside the open unit ball, but $\pi(\Gamma_1)$ does not necessarily lie outside the open unit disk. The shaded region in Figure 3.4 is one quarter of the unit disk.

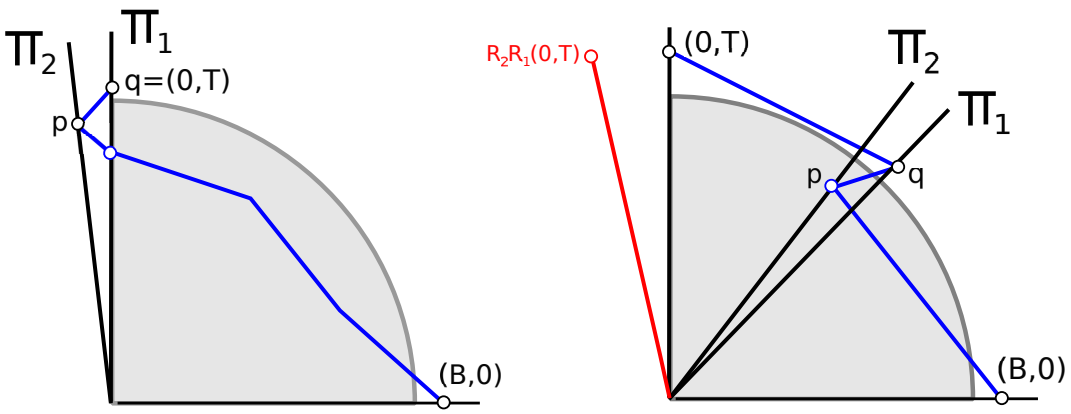

Figure 3.4: Projection of the ridge curve.

Let ℓ_1 denote the length of Γ_1. Let R_j denote reflection in Π_j. We write $\Gamma_1 = \Gamma_{11} \cup \Gamma_{12} \cup \Gamma_{13}$, where Γ_{11} goes from $(B, 0, 0)$ to p and Γ_{12} goes from p to q and Γ_{13} goes from q to $(0, T, 0)$.

The continuous path

$$\Gamma_1^* = \Gamma_{11} \cup R_2(\Gamma_{12}) \cup R_2R_1(\Gamma_{13})$$

has the same length as Γ_1 and connects $(B, 0)$ to $R_2R_1(0, T, 0)$. This latter point lies in the XY plane and makes an angle 2θ with the Y-axis, as shown (projected into the XY-plane) on the right side of Figure 7.2. But then

$$\ell_1 = |\Gamma_1^*| \geq (\pi/2) + 2\theta. \tag{6}$$

Let ℓ_2 denote the length of Γ_2, the portion of the ridge curve associated to τ_2. From Theorem 3.1 we have $\ell_1 < \sqrt{3} + (1/24)$. Combining this with Equation 6, we have

$$2\theta < \sqrt{3} + (1/24) - (\pi/2) < \pi/15. \tag{7}$$

Hence $\theta < \pi/30$. If one of our estimates failed, Γ_1 would make exactly the kind of path just studied, where the angle θ between Π_1 and Π_2 would be $\theta = \pi/30$. This is a contradiction. ♠

4 Tensegrities

4.1 Trapezoids and Capacities

We first mention a general property of our notation. For any object X in the plane X' will be the image of X under some kind of piecewise linear map to $\boldsymbol{R}^3$. Suppose that

$$Q = (Q_0, Q_1, Q_2, Q_3), \qquad Q' = (Q'_0, Q'_1, Q'_2, Q'_3)$$

are as follows: Q is a trapezoid in the plane having vertical sides and width 1 and Q' is a quadrilateral in $\boldsymbol{R}^3$. Figure 4.1 shows Q. The numbers indicate the labeling of the vertices of Q.

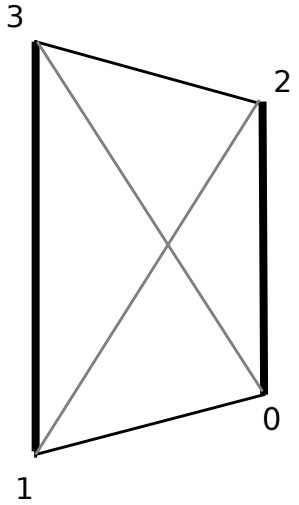

Figure 4.1: The quadrilateral tensegrity.

Let $d_{ij} = \|Q_i - Q_j\|$. Let $d'_{ij} = \|Q'_i - Q'_j\|$. We define the *height* of Q to be the sum of the vertical edge lengths of Q, namely $d_{02} + d_{13}$. We call the pairs (Q_0, Q_1) and (Q_2, Q_3) the *bends* and we call the pairs (Q'_0, Q'_1) and (Q'_2, Q'_3) the *bend images*. This lines up our discussion here with Figure 2.3.

We say that (Q, Q') is a *plain tensegrity pair* if $d_{ij} \geq d'_{ij}$ for all the edges of Q, with equality for the pairs $(0, 1)$ and $(2, 3)$. So, we have 2 equalities and 6 inequalities. We define the *capacity* of Q' to be the minimum height of Q where (Q, Q') is a tensegrity pair. We denote this by $\kappa(Q')$.

4.2 Compound Tensegrities

This time let $\Psi' = (Q'_0, ..., Q'_{k-1})$ be a collection of k quadrilaterals in space. We call k the *complexity*. We have

$$Q'_j = (Q'_{j,0}, Q'_{j,1}, Q'_{j,2}, Q'_{j,3}), \qquad j = 0, ..., (k-1).$$

We insist that these quads abut, in the sense that

$$Q_{j,2} = Q_{j+1,0}, \qquad Q_{j,3} = Q_{j+1,1}, \qquad j = 1, ..., (k-2).$$

When these conditions are satisfied, we call Ψ' a *compound tensegrity*. We will always take $k = 2$ here.

We call Ψ' *cyclic* if, additionally,

$$Q_{k-1,0} = Q_{0,1}, \qquad Q_{k-1,1} = Q_{0,0}. \tag{8}$$

The mismatch of the indices is deliberate, and is designed to reflect the structure of a Moebius band. When Ψ' we will take $k = 4$.

In either case, we define

$$\kappa(\Psi') = \sum_{i=0}^{k-1} \kappa(Q'_i). \tag{9}$$

Suppose now that (τ_1, τ_2) is a tame pair (or indeed any pair) of trapezoids coming from the process of cutting a polygonal Moebius band open along the bends corresponding to a T-pattern. Suppose we choose a finite number of additional bends $\beta_{1,1}, ..., \beta_{1,k_1-1}$ in the interior of τ_1 and $\beta_{2,1}, ..., \beta_{1,k_2-1}$ in the interior of τ_2. Then we can get a compound tensegrities in 3 ways:

- We set $\beta_{1,0} = b$ and $\beta_{1,k_1} = t$ and then let Q_j be the quadrilateral whose vertices are the endpoints of $I(\beta_1, j)$ and $I(\beta_1, j+1)$ with the vertices labeled as in Figure 4.1. Then $Q_0, ..., Q_{k_1-1}$ is a compound tensegity. Here b and t are the bottom and top bend of τ_1. Call this Ψ'_1.

- We set $\beta_{2,0} = t$ and $\beta_{2,k_2} = b'$ and then repeat the same construction. Here b' is the top of τ_2 which is parallel to b. Call this Ψ'_2.

- We can take the concatenation $\Psi' = \Psi'_1, \Psi'_2$ of the previous two tensegrities. This gives us a cyclic compound tensegrity.

Here is the key inequality:

$$S_1 \geq \kappa(\Psi'_1), \qquad S_2 \geq \kappa(\Psi'_2), \qquad \lambda(\tau_1, \tau_2) \geq \kappa(\Psi'). \tag{10}$$

4.3 The Essential Part

In some situations we will have occasion to work with a cyclic tensegrity of complexity 4 in which the first 3 trapezoids deserve to be considered on their own. We say that the *essential part* of the tensegrity is the union of these 3 trapezoids. When we consider the essential part, it will correspond to τ_1 and the remaining trapezoid will be τ_2. Here (τ_1, τ_2) is the tame pair associated to a polygonal Moebius band of aspect ratio less than $\sqrt{3} + 10^{-100}$ which has a T-pattern.

4.4 Reduced Capacity

We defined the capacity κ in terms of Figure 4.1. We define a simpler and potentially smaller invariant $\overline{\kappa}$ in terms of the tensegrity which ignores the diagonals. In other words, referring to the discussion surrounding Figure 4.1, we simply drop the requirement that $d_{ij} \geq d'_{ij}$ for $(i,j) = (1,2)$ and $(i,j) = (0,3)$. We have $\overline{\kappa} \leq \kappa$ and sometimes there is strict inequality. The invariant $\overline{\kappa}$ is much simpler than κ. We obviously have $\overline{\kappa} \leq \kappa$. Sometimes the inequality is strict and sometimes it is not. Algebraically, the reduced capacity is much nicer to work with. In most cases, it suffices to use the reduced capacity but in a few cases the results for κ are true by much wider margins than they are for $\overline{\kappa}$.

5 The Topology Lemma

In this chapter we reduce the Topology Lemma to tensegrity calculations. We first prove the Topology Lemma under a condition we call *Topological Goodness*. Following this, we reduce topological goodness to a property we call *Geometrical Goodness*, a purely geometric property. We then reduce Geometrical Goodness to tensegrity calculations.

5.1 Topological Goodness

Given 2 bends β_1 and β_2 we write $\beta_1|\beta_2$ if β_1^* and β_2^* intersect in a point that is interior to both. Assuming that $\beta_1|\beta_2$, we write $\beta_1 \uparrow \beta_2$ if the vertical line through $\beta_1^* \cap \beta_2^*$ intersects $I(\beta_1)$ above where it intersects $I(\beta_2)$. Otherwise we write $\beta_1 \downarrow \beta_2$. We must have one or the other when we have an embedded Mobius band. We will encode the information below in a picture reminiscent of a knot diagram.

We call $(\beta_1, \beta_2, \beta_3)$ a *topologically bad triple* triple if the crossings are inconsistent in one of two ways:

- $\beta_1 \uparrow \beta_2$ and $\beta_1 \downarrow \beta_3$.
- $\beta_1 \downarrow \beta_2$ and $\beta_1 \uparrow \beta_3$.

Otherwise we call the triple *topologically good*.

Good Pairs: We say that the pair (τ_1, τ_2) is *topologically good* if:

1. $(0)|(4)_j$ and $(1)_1|(4)_j$ and $(4)_1|(4)_2$.
2. $(4_j, 1_1, 0)$ is topologically good.
3. $(1_1, 4_j, 6)$ is topologically good unless $\tau_j \to_1 \tau_i$.
4. $(4_{3-j}, 4_j, 0)$ is topologically good unless $\tau_j \to_4 \tau_{3-j}$.

Here $j = 1, 2$ in all statements.

Our next result proves the Topology Lemma under the assumption that we have a topologically good pair. The basic idea is that various topological crossing diagrams are impossible under the assumptions above, and this forces the desired incidences.

Lemma 5.1 *The Topology Lemma holds for topologically good pairs.*

Proof: Suppose first that $(1)_1^*$ and 6^* do not cross. Since $(1)_1|(4)$, there is by continuity some $\beta \in [4,6]_1$ such that β^* contains the 1-tip of $(1)_1^*$. This means that $\tau_1 \to \tau_1$.

Henceforth we assume $(1)_1|(6)$. We normalize by an ambient isometry so that $(1)_1 \downarrow (6)$. Figure 5.1 shows the 4 possibilities.

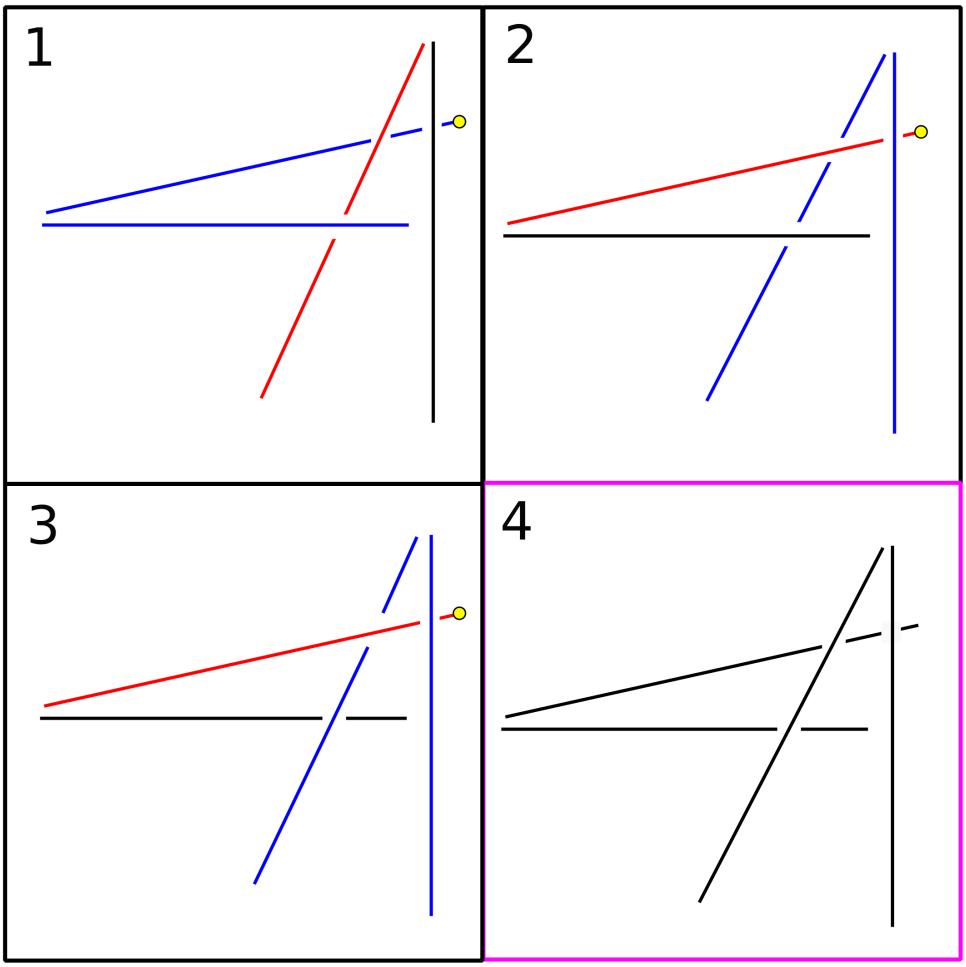

Figure 5.1: Four possibilities

Case 1 has the topologically bad triple $(4_1, 1_1, 0)$, so this case cannot happen. Cases 2 and 3 have the topologically bad triple $(1_1, 4_1, 6)$. Hence $\tau_1 \to_1 \tau_1$ in these cases. This leaves Case 4.

Let us explore Case 4 in more detail. Figure 5.2 shows the situation.

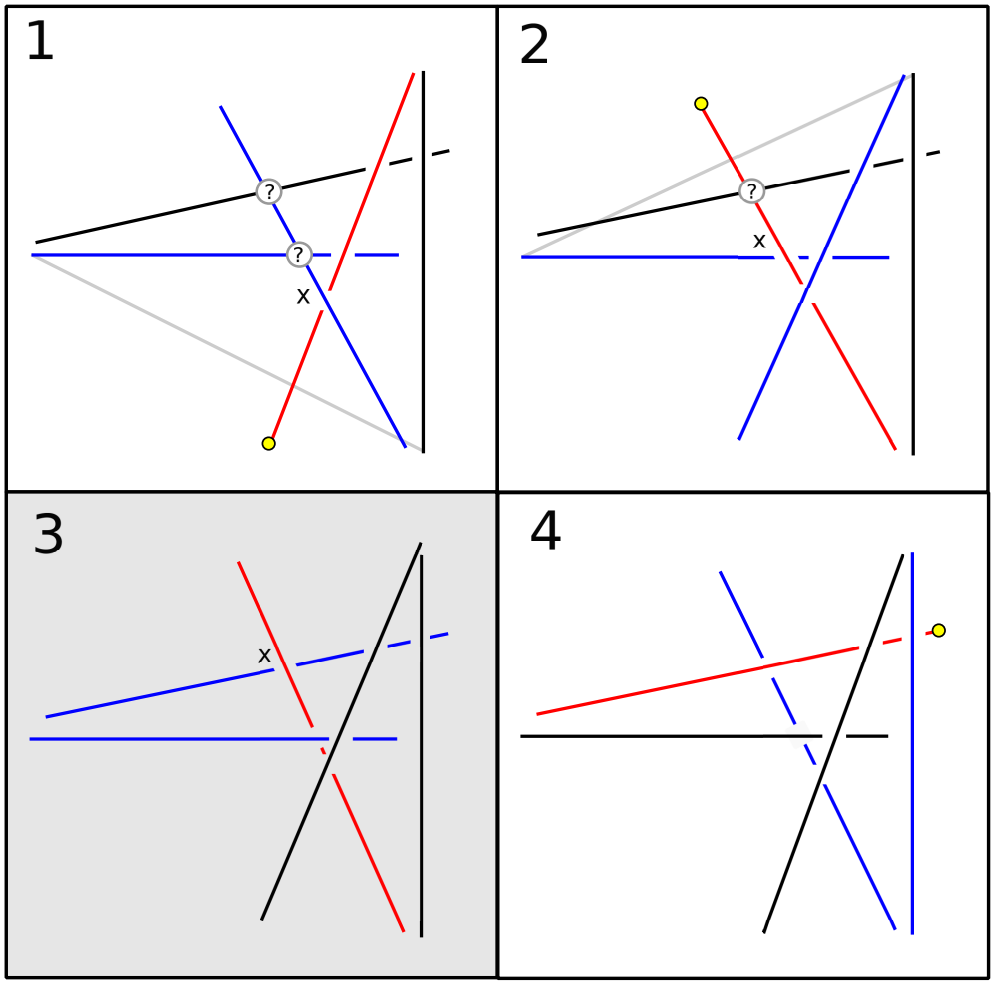

Figure 5.2: Four possibilities

In Case 1 we have left 2 crossings undetermined and we place an x by the crossing we study. If the crossing is as appears, then $(4_1, 4_2, 0)$ is a topologically bad triple. But then $\tau_2 \to_4 \tau_1$.

In Case 2 we are working on the next crossing, and we still leave one undetermined. This has the same structure as Case 1 but with the indices 1 and 2 reversed. Hence $\tau_1 \to_4 \tau_2$ here.

In Case 3, the situation is impossible because $(4_2, 1_1, 0)$ is a topologically bad triple.

In Case 4, the triple $(1_1, 4_2, 6)$ is topologically bad. Hence $\tau_2 \to_1 \tau_1$. ♠

5.2 Geometrical Goodness

Here we give conditions under which the pair (τ_1, τ_2) is topologically good. We call the triple $(\beta_1, \beta_2, \beta_3)$ of bends *geometrically good* if $\beta_1 | \beta$ for all bends β that interpolate between β_2 and β_3. Since the space of bends is topologically a circle, we we have to be careful about what we mean here. We never allow our bends in an interpolating family to cross the bend labeled T on the left side of Figure 2.1. In the next result, we have our standard normalization. We call (τ_1, τ_2) *geometrically good* if the various conditions on the triples in the definition of topological goodness hold with the word *geometrically* replacing the word *topologically* in every instance.

Lemma 5.2 *(τ_1, τ_2) is topologically good if (τ_1, τ_2) is geometrically good.*

Proof: For a given triple, the implication "geometric implies topological" works the same way in all cases. We just consider two representative cases.

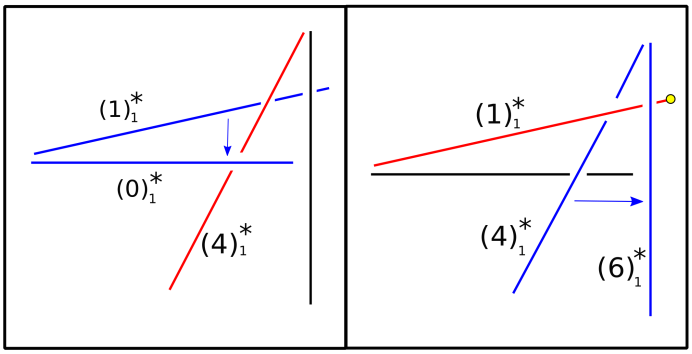

Figure 5.3: A topological contradiction.

First look at the left half of Figure 5.3. Consider the triple $(4_1, 1_1, 0)$. In $\boldsymbol{R}^3$, as we sweep the blue $I(I_1)$ over to the blue $I(0)$ we end up on the wrong side of the red $I(4_1)$. The geometrical goodness prevents the crossing type from changing.

Now look at the right half of Figure 5.3. As we sweep the blue $I(4_1)$ over to the blue $I(6)$, we get the same contradiction as in the previous case, except that now the crossing can change if the projection of one of the blue segments in our sweepout contains the right endpoint of $(1)^*_1$. In other words, $(1_1, 4_1, 6)$ is topologically good unless $\tau_1 \to_1 \tau_1$. ♠

5.3 The Cyclic Tensegrities

Our approach to establishing geometrical goodness involves 2 calculations with cyclic tensegrities of complexity 4 and a whole bunch of calculations with compound tensegrities of complexity 2. We first explain the two cyclic tensegrities of complexity 4. Since we will have occasion to use similar calculations for the Geometry Lemma, we will introduce a somewhat general framework.

We describe 2 closely related families of complexity 4 cyclic tensegrities. The input for both families is an index $h \in \{0,1\}$ and a pair Θ_1, Θ_2 of (angle) intervals as in the proof of Lemma 3.2. One of the angle intervals is a point and one is a nontrivial interval.

We use the notation from the previous chapter, so that $\{Q_{ij}\}$ is the list of points in the domain and $\{Q'_{ij}\}$ is the list of points in the range. We have the *bend images*

$$\beta'_j = \overline{Q'_{j,0}Q'_{j,1}}$$

for $j = 0,1,2,3$. Let π be projection into the XY-plane. Recall that the *pitch* of β' is the angle that $\pi(\beta')$ makes with the X-axis.

The family $\mathcal{F}(h, \Theta_1, \Theta_2)$ is the set of tensegrities such that:

- $\beta'_0 \cup \beta'_3$ is a T-pattern, with $\pi(\beta'_0)$ horizontal and $\pi(\beta'_3)$ vertical.
- β'_j has pitch in the interval Θ_j for $j = 1,2$.
- $\pi(\beta'_2)$ contains the point $\pi(Q_{1,h})$.

This family corresponds to a situation where we focus on two auxiliary bends both lying in the trapezoid τ_1, the lower half of our polygonal Moebius band. For later use, we define the *essential part* of a member of $\mathcal{F}$ to be the complexity 3 tensegrity made from the union of the bottom 3 trapezoids. The essentially part corresponds to τ_1.

The family $\mathcal{G}(j, \Theta_1, \Theta_3)$ is defined in the same way as $\mathcal{F}$ except that the indices 2 and 3 are swapped. Thus, for instance $\beta'_0 \cup \beta'_2$ make a T-pattern. The $\mathcal{F}$ encodes the situation where we focus on two bends contained in τ_1 and the family $\mathcal{G}$ encodes the situation where we focus on two bends, one contained in τ_1 and the other contained in τ_2.

Now we mention the two calculations. Each of these calculations involves the positivity of some 14-dimensional piecewise algebraic expression.

1. All members of $\mathcal{F}(0, [4\pi/12, 4\pi/12], [-\theta_0, +\pi/12], 4\pi/12)$ have reduced capacity greater than $2\sqrt{3}$.

2. All members of $\mathcal{G}(0, [4\pi/12, 4\pi/12], [-\pi/12, +\theta_0], 4\pi/12)$ have reduced capacity greater than $2\sqrt{3}$.

Figures 5.4 and 5.5 represent two members of each family described above.

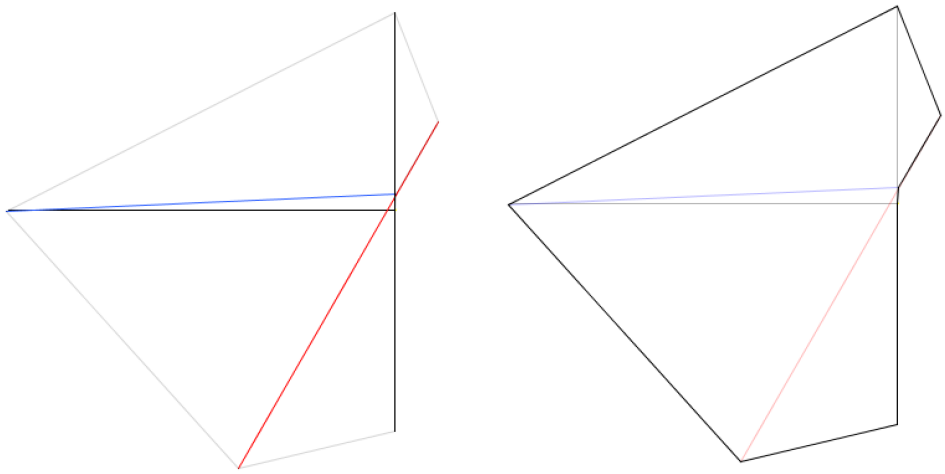

Figure 5.4: The Constraints for Cyclic Calculation 1.

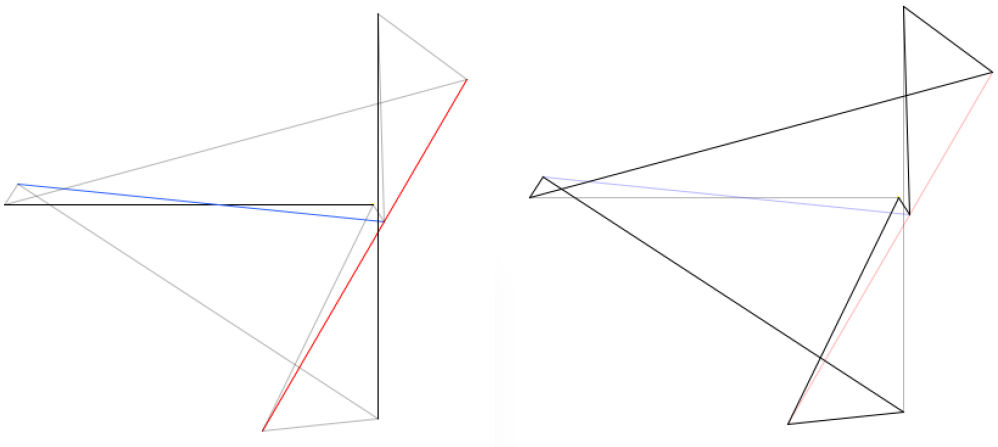

Figure 5.5: The Constraints for Cyclic Calculation 2.

5.4 The Compound Tensegrities

Now we discuss the remaining tensegrity calculations. These involve compound tensegrities of complexity 2.

A *prism* is a set of the form $P \times \boldsymbol{R}$, where $P \subset \boldsymbol{R}^2$ is an open convex polygon. The prism is the intersection of finitely many halfspaces whose boundaries project to lines in the XY-plane. We call these halfspaces the *defining halfspaces*. In general, we say that a halfspace whose boundary projects to a line in the XY-plane is a *prism halfspace*.

Our calculations all involve compound tensegrities with 2 quadrilaterals. Given such a tensegrity Υ', we let $\theta(\Upsilon')$ denote the pitch of the middle bend image $\overline{Q'_{10}Q'_{11}}$. Here are the constraints.

1. The horizontal and vertical bends make a T-pattern.
2. $\theta(\Upsilon') \in \Theta \subset [-\theta_0, \pi/2 + \theta_0]$, for some interval Θ.
3. A selected endpoint of the middle bend lies in the prism halfspace H.

Again, $\theta_0 = \pi/30$ as in Lemma 3.2.

For various choices of (Θ, H) the calculations, if valid, show

$$\kappa(\Upsilon') > \sqrt{3} + \frac{1}{24} + 10^{-100}.$$

We call (j, Θ, H) an *excluder*. Suppose that (j, Θ, H) is an excluder. Suppose (τ_1, τ_2) is a tame pair and $I(\beta)$ is a bend image associated to τ_1 having pitch in Θ. Then the relevant endpoint of $I(\beta)$ cannot lie in H. Here is the argument. The calculation above, applied to $\Upsilon' = \Psi'_1$, shows that if this fails then $S_1 > \sqrt{3} + \frac{1}{24} + 10^{-100}$. On the other hand, Theorem 3.1 gives us that $S_2 > \sqrt{3} - \frac{1}{24}$. But then $\lambda(\tau_1, \tau_2) > \sqrt{3} + 10^{-100}$, contradicting tameness.

Confining Pairs: We say that a *prism pair* is a pair (P_1, P_2) of disjoint prisms. We say that this pair *confines* a line segment if one endpoint of the line segment lies in P_1 and the other lies in P_2. Let $H_{j,1}, ..., H_{j,k_j}$ be the closed complements of the defining halfspaces for P_j. For fixed Θ we set up calculations which would show that $(j, \Theta, H_{j,i})$ is an excluder for all relevant indices. This shows that (P_1, P_2) confines the middle bend image $I(\beta)$ associated to (τ_1, τ_2) provided that and pitch θ of the middle bend lines in Θ. We abbreviate this by saying that (P_1, P_2) is a Θ *confiner*.

The Main Examples: Now we describe the Confiner Calculations we need in order to establish Geometrical Goodness. In all cases we use the ordinary capacity (as opposed to the reduced capacity).

Figure 5.6 shows 6 regions in the plane. These regions are projections of prism pairs. The red and green regions are interchanged by reflection in the X-axis. As always, we show the projection to the XY-plane. The circle in the picture denotes a place where the pieces are actually disjoint but look tangent. The green piece is entirely below the line extending the bottom edges of the blue piece.

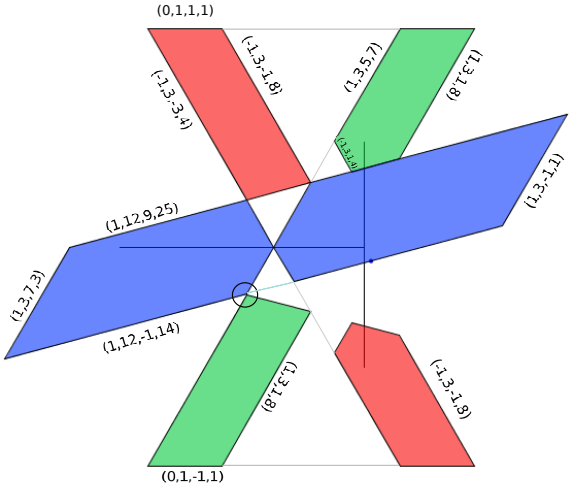

Figure 5.6: Confining prisms

Figure 5.7 shows some new regions. The blue regions in Figure 5.7 are the same as in Figure 5.6. The magenta regions are reflections of the blue regions in the X-axis.

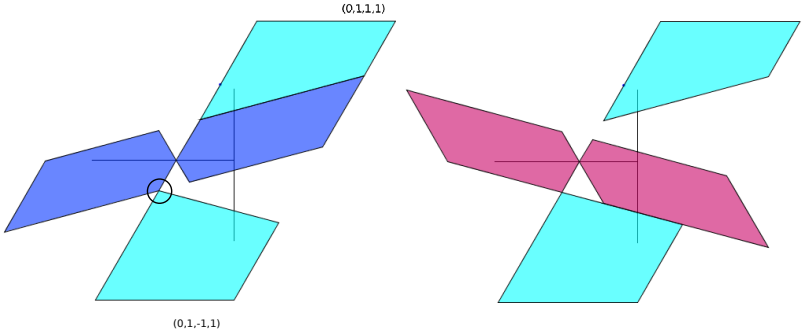

Figure 5.7: Confining prisms

The red regions in Figure 5.8 are the same as in Figure 5.6.

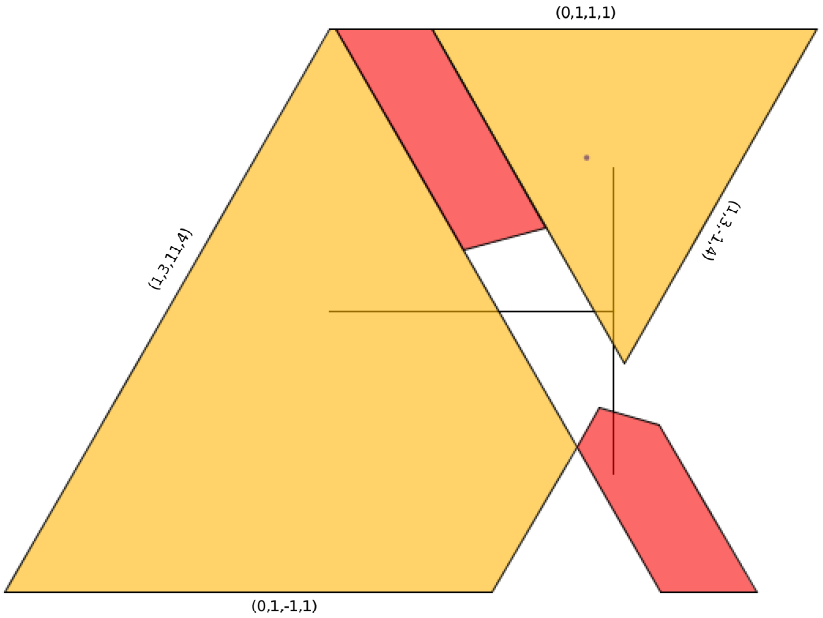

Figure 5.8: Confining prisms

Motivated by Lemma 3.2, we define

$$\Theta_{01} = [-\theta_0, \pi/12], \quad \Theta_{44} = [4\pi/12, 4\pi/12],$$

$$\Theta_{46} = [4\pi/12, 6\pi/12 + \theta_0], \quad \Theta_{04} = [-\theta_0, 4\pi/12 + \theta_0]. \tag{11}$$

The notation is such that $\Theta([i,j]_1) \subset \Theta_{ij}$. Here are the calculations.

1. The green prisms are a Θ_{44} confining pair.
2. The blue prisms are a Θ_{01} confining pair.
3. The cyan prisms are a Θ_{46} confining pair.
4. The orange prisms are a Θ_{04} confining pair.

5.5 Establishing Geometrical Goodness

Now we deduce Geometrical Goodness from the truth of the calculations above.

Lemma 5.3 *The triple* $(4_1, 1_1, 0)$ *are geometrically good.*

Proof: Our argument refers to Figure 5.6. Call a segment *red* if it has one endpoint in the interior of one red region and the other endpoint in the interior of the other. Likewise define *green segments* and *blue segments*. Looking at Figure 5.6, we see that a green segment fails to cross a blue segment only if the line extending the green segment lies to the right of the entire blue segment.

At the same time, the conclusions from Cyclic Calculation 1 say that the right endpoint of a blue segment cannot lie in the line extending a green segment. The green segment is always $(4)_1^*$ and the blue segment can be any β^* with $\beta \in [0,1]_1$. But β^* varies continuously. Hence, from what we have already said, either β^* crosses $(4)_1^*$ for all choices of β or for none of them. But $(0)^*$, which is just the horizontal bend, definitely crosses the green segment. Hence all the blue segments cross the green segment. This shows that $(4_1, 1_1, 0)$ is geometrically good. ♠

Corollary 5.4 *The triple* $(4_2, 1_2, 0)$ *is geometrically good.*

Proof: This follows from the previous case and symmetry. We just interchange the roles played by the indices. ♠

Lemma 5.5 *The triple* $(4_2, 1_1, 0)$ *is geometrically good.*

Proof: This is the same argument as in the proof for $(4_1, 1_1, 0)$ except that we use *red* in place of *green* and Cyclic Calculation 2 in place of Cyclic Calculation 1. Note that Cyclic Calculation 2 gives bounds on the bend 4_1 and also the bends in $[0,1]_2$ rather than the bend 4_2 and the bends $[0,1]_1$. so we really are using the statement that is exactly like the Cyclic Calculation 2 except with the roles of the indices interchanged. ♠

Corollary 5.6 *The triple* $(4_1, 1_2, 0)$ *is geometrically good.*

Proof: Symmetry. ♠

Summarizing the results above, we see that $(4_i, 1_j, 0)$ is good for all indices $i, j \in \{1, 2\}$.

Lemma 5.7 $(1_i, 4_j, 6)$ *is geometrically good unless* $\tau_j \to_1 \tau_i$.

Proof: By symmetry, it suffices to take $j = 1$. This time our argument refers to Figure 5.7. Looking at Figure 5.7, we see that a blue segment crosses a green segment unless the line extending the green segment lies to the right of the blue segment. We have already shown that $(1)_1^*$ and $(4)_1^*$ cross. Consider the continuous family of segments of the form β^*, where β sweeps through $[4, 6]_1$. The first segment crosses $(1)_1^*$. Therefore, from what we have observed about blue and green segments, either every β^* crosses $(1)_1^*$, or one of them contains the right endpoint of $(1)_1^*$. In this latter case, we have $\tau_1 \to_1 \tau_1$ by definition. Hence $(1_1, 4_1, 6)$ is geometrically good unless $\tau_1 \to_1 \tau_1$.

By symmetry, any segment of the form β^* with $\beta \in [0, 1]_2$ is magenta. The same argument as above, with *magenta* replacing *blue*, implies that $(1_2, 4_1, 6_1)$ is good unless $\tau_1 \to \tau_2$. ♠

In this result we take $i \neq j$.

Lemma 5.8 *The triple* $(4_i, 4_j, 0)$ *is geometrically good unless* $\tau_j \to_4 \tau_i$.

Proof: If suffices to take $i = 2$ and $j = 1$. Our argument refers to Figure 5.8. Note that an orange segment always crosses a red segment unless that line extending the orange segment lies above the red segment. We have already seen that $4_1|4_2$. The same argument as in the previous lemma shows that $(4_2, 4_1, 0)$ is geometrically good unless $\tau_1 \to_4 \tau_2$. ♠

This covers all triples we need to consider in order to establish Geoemtrical Goodness for a tame pair (τ_1, τ_2) of trapezoids. This completes our reduction of the Topology Lemma to tensegrity calculations.

6 The Geometry Lemma

6.1 Three Cyclic Tensegrity Calculations

We first describe an approach which does not quite work. The following three calculations imply the Geometry Lemma.

- The essential part of every element of $\mathcal{F}(0, \pi/12, [4\pi/12, 6\pi/12 + \theta_0])$ has reduced capacity at least $\sqrt{3}$. Equality occurs only when the convex hull of the T-pattern is an equilateral triangle of perimeter $2\sqrt{3}$.
- Every element of $\mathcal{G}(1, -4\pi/12, [-\theta_0, \pi/2])$ has reduced capacity at least $2\sqrt{3}$. Equality occurs only when the convex hull of the T-pattern is an equilateral triangle of perimeter $2\sqrt{3}$.
- Every element of $\mathcal{G}(0, \pi/12, [6\pi/12 - \theta_0, 8\pi/12])$ has reduced capacity at least $2\sqrt{3}$. Equality occurs only when the convex hull of the T-pattern is an equilateral triangle of perimeter $2\sqrt{3}$.

I call these statements Calculations 1,2 and 3'. Figure 6.1-6.3 show typical members of each of the families above. On the left hand side of each picture, we are emphasizing the bend images. On the right hand side, we are emphasizing a kind of perimeter. The length of the black curve on the right is less or equal to the reduced capacity of the corresponding tensegrity.

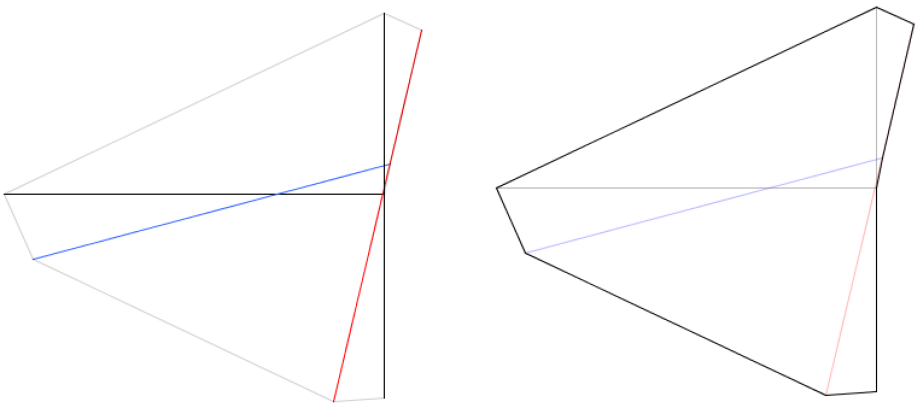

Figure 6.1: The constraints for Calculation 1

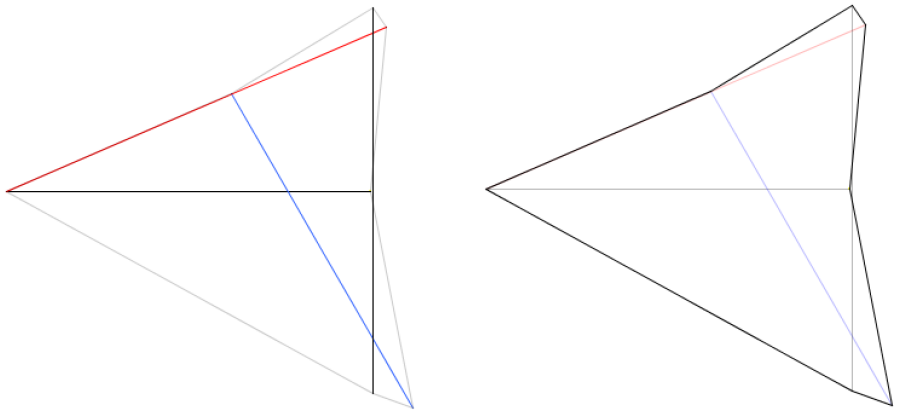

Figure 6.2: The Constraints for Calculation 2

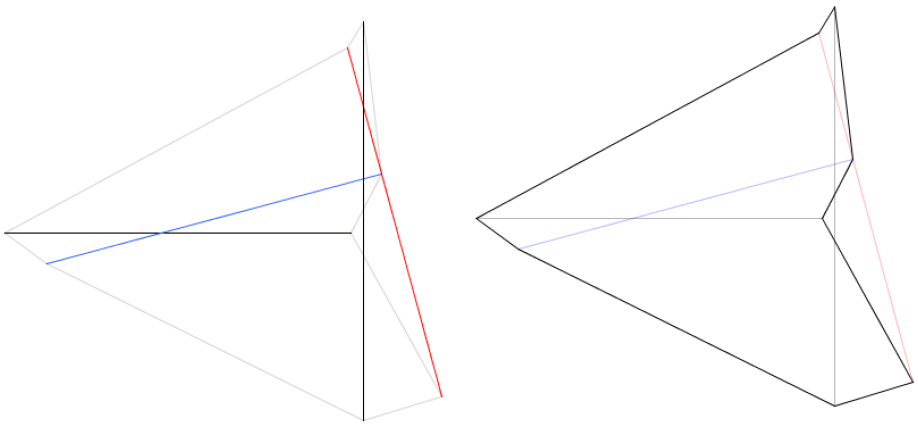

Figure 6.3: The Constraints for Calculation 3'

After a lot of experimentation, I think that Calculations 1 and 2 work. The inequalities really are true. (I would not bet my life on it, however.) Calculation 3', if true, would take care of Cases 3 and 4 of the Geometry Lemma at the same time. Unfortunately, Calculation 3 does not work. I found members in the family above which have capacity less than $2\sqrt{3}$. When I use the reduced capacity these are easier to find, but they also occur with the non-reduced capacity.

A variant of Calculation 3' seems to work. The capacity of the essential parts of members of $\mathcal{G}(...)$ seems always greater than $\sqrt{3}$. Unfortunately, the third trapezoid is associated to τ_2 and not τ_1, and this estimate would not help us even if true.

6.2 The Last Two Calculations

The last two calculations, which I call Calculations 3 and 4, involve more complicated tensegrities. They are the replacement for the failed Calculation 3'. Since I have not yet coded these up yet, I will just explain these calculations schematically. To rule out the possibility that $\tau_1 \to_1 \tau_2$ and $\tau_2 \to_1 \tau_1$ we work with a cyclic tensegrity of complexity 6 tensegrity, as suggested by Figure 6.4.

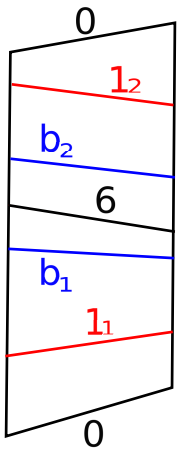

Figure 6.4: Schematic picture for Calculation 3

In the tensegrity, the following conditions hold:

- The bends labeled 0 and 6 correspond to the T-pattern, as in all the other tensegrities.
- The bends labeled 1_1 and 1_2 correspond to bend images which have pitch $\pi/12$ and $-\pi/12$ respectively.
- The bends labeled b_1 and b_2 correspond to bend images which have pitch in the intervals $[4\pi/12, 6\pi/12 + \theta_0]$ and $[6\pi/12 - \theta_0, 8\pi/12]$ respectively.
- The right endpoint of 1_1^* lies in b_2^*. These are the planar projections of the corresponding bend images.
- The right endpoint of 1_2^* lies in b_1^*. These are the planar projections of the corresponding bend images.

In a sense this tensegrity is like two interlocking copies of the tensegrity for Calculation 3' above. The calculation we would hope to make is that any tensegrity like this has capacity at least $2\sqrt{3}$, with equality if and only if the configuration corresponds to the presumed optimizer.

Now I will explain schematically how to rule out that possibility that $\tau_1 \to_1 \tau_1$ and $\tau_1 \to_1 \tau_2$. Figure 6.5 shows a picture like the one in Figure 6.4, except that ordering of the bends and the incidence relations are a bit different.

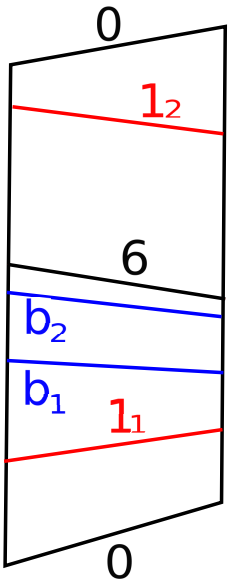

Figure 6.5: Schematic picture for Calculation 4.

There are actually 3 different tensegrity patterns we would need to consider.

- The right endpoint of 1_i^* lies in b_i^* for $i = 1, 2$.
- The right endpoint of 1_{3-i}^* lies in b_i^* fo $i = 1, 2$.
- $b_1 = b_2 = b$ and the right endpoints of 1_i^* lie in b^* for $i = 1, 2$.

7 Numerical Computations

7.1 Parametrizing Tensegrities

For our calculations we want to parametrize the set of all tensegrities which satisfy certain constraints. There is a tradeoff between the simplicity of the parametrization and the efficiency of the calculation. The simplest approach is just to string out all the coordinates of the vertices and realize the set of interest to us as a subset of a giant and high dimensional cube. This leads to very inefficient calculations. We describe a more complicated approach which does better.

We define

$$\iota(a,b,r) = (1-r)a + rb. \tag{12}$$

We can think of $\iota(a,b,*)$ as being a map from $[0,1]$ to the interval $[a,b]$. We will use this map repeatedly.

The Bends: The tensegrities we consider have either 3 or 4 bend images Let us say that there are $\ell+1$ bend images, $\beta_0,...,\beta_\ell$. So, we have $\ell=2$ or $\ell=3$. We arrange the indices so that $j=0$ and $j=\ell$ correspond to the horizontal and vertical bend images.

Given a point $(r_0,...,r_\ell) \in [0,1]^{\ell+1}$ we set

$$s_0 = \iota(0,1/2,r_0), \qquad s_j = \iota(-1,1,r_j), \;\; j=1,...,\ell,$$

$$s_\ell = \iota(a(s_0), b(s_0), r_\ell). \tag{13}$$

Here $a(s_0)$ and $b(s_0)$ are obtained as follows. We intersect the vertical line $x=s_0$ with the quadrilateral $\widehat{\Omega}$ from Theorem 3.1 and take the upper and lower limits. The precise formulas are

$$a(s_0) = (2/3)s_0 - (1/\sqrt{3}), \quad b(s_0) = \min(b_1(s_0), b_2(s_0)),$$

$$b_1(s_0) = \min((2/3)s_0 - (1/2), \quad b_2(s_0) = (4/3)s_0 - (1/\sqrt{3})). \tag{14}$$

In our definition of s_0 we could take $s_0 \in [0, \frac{1}{4}(\sqrt{27}-\sqrt{11})]$, but it is simpler just to take $s_0 \in [0,1/2]$. In terms of Figure 2.1, we are setting $b=s_0$ and $t=s_k$.

This approach allows (s_0,s_ℓ) to sample all of $\widehat{\Omega}$. The other bend slopes $s_1,...,s_{k-1}$ are each allowed to lie in $[-1,1]$, which certainly covers all the possibilities. Referring to Figure 2.1, we have $b=s_0$ and $b=s_\ell$.

The Offsets: Given $(r_1, r_2) \in [0,1]^2$ we define

$$x = \iota(0, 1/18, r_1), \qquad y = \iota(-1/30, 1/30, r_2). \tag{15}$$

These are the coordinates of the vector shown in Figure 2.1.

The coordinates (b, t, x, y) determine the placement of the horizontal and vertical bend images. The horizontal bend image is the segment with endpoints $(0,0)$ and $(-\sqrt{1+b^2}, 0, 0)$. The vertical bend image is centered at (x, y) and has length $\sqrt{1+t^2}$.

Confiner Calculations: For the Confiner Calculations it only remains to describe how we parametrize the middle bend. The parameter s_1 determines the length of this bend. Given a point $(r_1, r_2, r_3, r_4, r_5) \in [0,1]^5$ we set

$$m_j = \iota(-1, 1, r_j), \;\; j = 1,2,3, \quad \theta = \iota(\theta_1, \theta_2, r_4), \quad \phi = \iota(-\pi/4, \pi/4.r_5). \tag{16}$$

Here (m_1, m_2, m_3) is the center of the middle bend. The interval $[\theta_1, \theta_2]$ is the pitch range for the middle bound. The angle ϕ is the angle that the middle bend image makes with the XY-plane.

So a point in $[0,1]^3 \times [0,1]^2 \times [0,1]^5 = [0,1]^{10}$ completely specifies any tensegrity of this type we need to consider.

The Simpler Geometry Calculations: In this case we have two middle bend images to worry about, β_1' and β_2'. We first describe our parameterization for tensegrities which lie entirely in the XY-plane and then we describe how we use 4 more parameters to give examples in $\boldsymbol{R}^3$.

We have already specified the lengths of the middle 2 bends. We just have to specify their pitch and center. The pitch of β_1' is given by the problem, and a point in $[0,1]^2$ gives the center. We use another copy of $[0,1]^2$ for β_2'. The first coordinate determines which point of β_2' contains the relevant endpoint of β_1'. The second coordinate determines the pitch. The pitch θ lies in some interval. Here are the choices we make.

1. In Geometry Calculation 1 we take $\theta \in [3\pi/10, 8\pi/15]$.

2. In Geometry Calculation 2 we take $\theta \in [5\pi/12, 7\pi/12]$.

3. In (the failed) Geometry Calculation 3' we take $\theta \in [1\pi/12, 3\pi/12]$.

In the first case, the angle interval is specified by the problem. In the second and third cases, the angle range is allowed to be arbitary buty our intervals above are not covering all the cases. However, our choices cover all the cases which, numerically, are fairly close. When we go outside the given ranges, the capacity is huge.

So, a point in $[0,1]^4 \times [0,1]^2 \times [0,1]^2 \times [0,1]^2 = [0,1]^{10}$ specifies a tensegrity image that lies in the XY-plane. To get a fully spatial example, we add 4 more variables. Note that in an example of minimal capacity, some point of β_1' lies in the XY-plane. (Otherwise we can decrease the capacity by a vertical adjustment.) A parameter in $[0,1]$ determines a point of β_1' and another parameter in $[0,1]$ determines how much we rotate β_1' in the vertical direction about this point. We make the tilt such that the tilt angle ϕ lies in $[-\pi/4, \pi/4]$. The same story goes for β_2'. Thus, a point $[0,1]^4$ gives the data we need to turn our planar example into a spatial example. All in all, $[0,1]^{14}$ specifies all relevant tensegrities.

Topology Calculations: Our parametrization for two Topology Calculations is just like the one for the Geometry Calculations, except that the pitch of the second of the middle bend images is fixed and the pitch of the first of the middle bend images varies within an interval. These intervals are specs of the problem, In both cases the interval is $[-\pi/30, \pi/12 + \pi/30]$.

The Complicated Geometry Calculations: The Geometry Calculations 3 and 4 involve higher complexity cyclic tensegrities. We would parametrize these above, and the huge unit cube $[0,1]^{26}$ would parametrize all the relevant tensegrities in each case.

7.2 Hill Climbing Algorithms

For all our calculations we have our capacity function $\kappa : [0,1]^N \to \boldsymbol{R}_+$. Here $N = 10$ for the Confiner Calculations and $N = 14$ for the Geometry and Topology Calculations. We have some lower bound λ and we are trying to show that

$$\min_{[0,1]^N} \kappa \geq \lambda. \tag{17}$$

More precisely, with our numerical calculations we are searching for possible counter-examples to this inequality and we want the most efficient way of finding them. If we don't find any counter-examples after running an efficient

optimizing algorithm for a reasonably long time, we guess that there are no counter-examples – i.e., the inequality is true.

We start with some initial point $r_0 \in [0,1]^N$. We then pick a small random step size s and a random point $r_1 \in [-1,1]^N$. We then replace r_0 by $(1-s)r_0 + sr_1$. If some coordinate of r_1 is negative, we set that coordinate equal to 0. If some coordinate of r_j exceeds 1, we set it equal to 1. In other words, we take a small step in a random direction and then retract to $[0,1]^N$ if necessary. If $f(r_1) < f(r_0)$ we replace r_0 with r_1 and repeat. This produces a sequence of points $r_0, r_1, r_2, ...$ on which κ is decreasing. The hope is that this sequence converges to a global minimum.

This algorithm is a reasonable approximation to Newton's method. At least at points where κ is smooth, a small step in a random direction has a 50 percent change of moving in the direction of the gradient. and a somewhat lower but still decent chance of making a small angle with the gradient. There is a long list of more sophisticated numerical optimization problems, and I will probably implement something better and report on it later on when I have done so.

For the Geometry and Topology Calculations, I also run a variant of the hill-climbing algorithm. With a small probability, say 10^{-6}, the algorithm moves to a new random location regardless of whether the function value is lower at the new location. This allows the algorithm to sample many potential basins of attraction. Let me call this approach *annealing*, though a true annealing argument is more sophisticated than this.

7.3 The Confiner Calculations

The idea behind the Confiner Calculations is quite simple. In order for the given point to lie outside the given prism halfplane, the tensegrity has to be "stretched" a lot. The stretching bumps up the capacity beyond $\sqrt{3}+(1/24)$. Figure 6.1 illustrates this with two examples. The first example shows a tensegrity near the minimum for the given constraint. The capacity here is about $\sqrt{3} + 0.14$. The second example shows a much more radical stretch, where the capacity is about $\sqrt{3} + 1.5$. The red edges correspond to the vertical sides of the associated planar quadrilaterals.

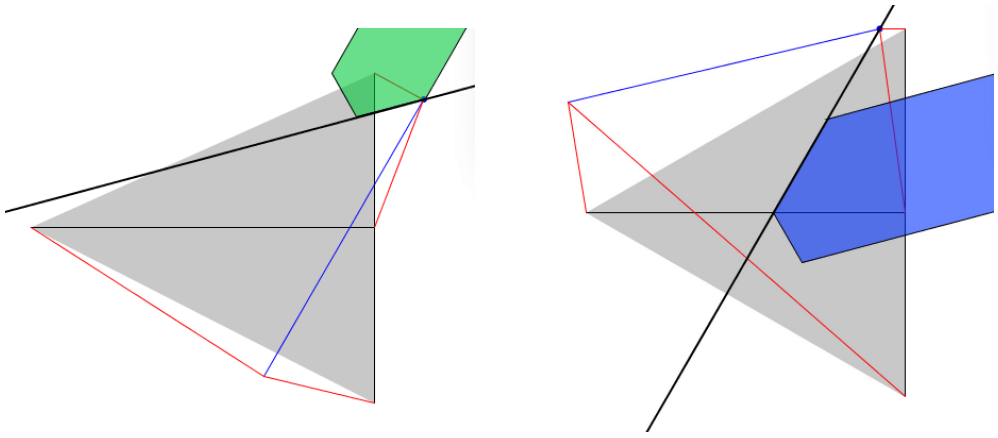

Figure 6.1: Calculation Records

Figures 6.2-6.3, which correspond to Figures 5.4-5.6 (with redundant pieces removed) give some idea of what the calculations are like. An edge labeled by, say, 0.1, indicates that after running the algorithm for a while with respect to the line extending the edge we conclude that the minimum of the capacity function is at least $\sqrt{3}+0.1$. Our target is $\sqrt{3}+(1/24) < \sqrt{3}+0.05$, so even in this case we have a healthy margin for success. The red lines indicate the most delicate calculations, and the orange lines indicate the next more delicate calculations. Everything else is pretty crudely true. I ran each of the calculations associated to the red edges at least 2 hours, and I ran the ones associated to the small red edge labeled 0.09 for about 8 hours.

There is something I want to say about the calculation where the bound is 0.08. (Actually it is closed to .09.) When I run this calculation I notice that when κ tends towards its minimum, the corresponding b value (the slope of the bottom bend) tends to the upper bound $(\sqrt{27}-\sqrt{11})/4$. This accounts for the elongated appearance of the grey triangle on the left side of Figure 6.1. If we wanted, we could do additional calculations to strengthen Statement 3 of Theorem 3.1 to say that we must have $b < 1/3$ whenever we have a tame pair (τ_1, τ_2). This would give us a more robust calculation result in this case.

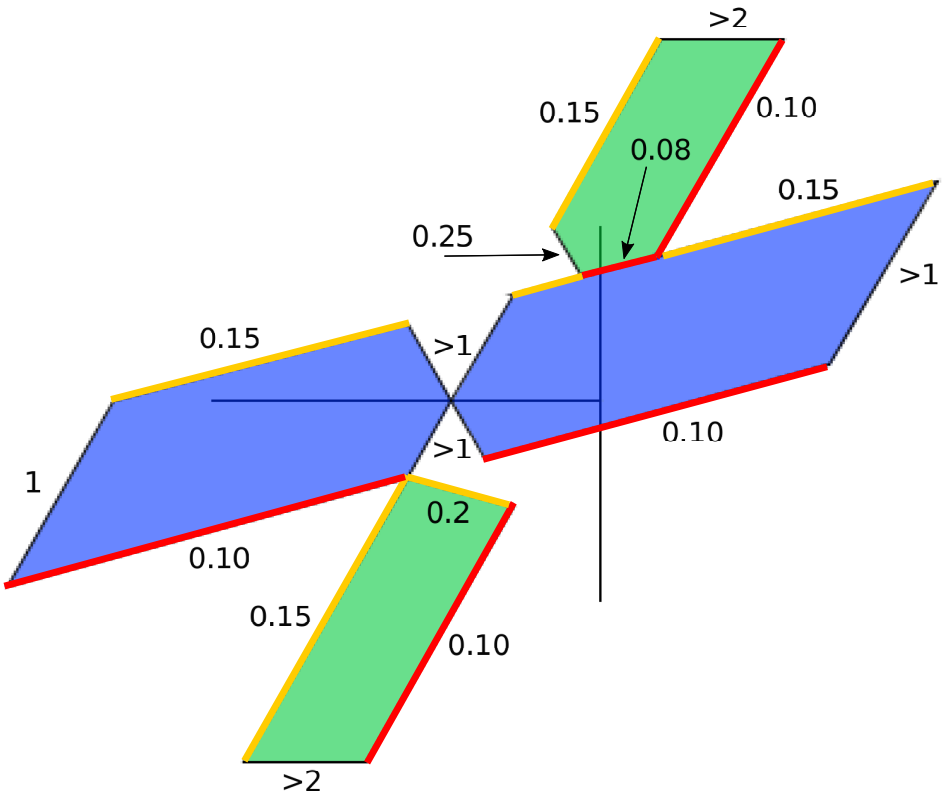

Figure 6.2: Calculation Records

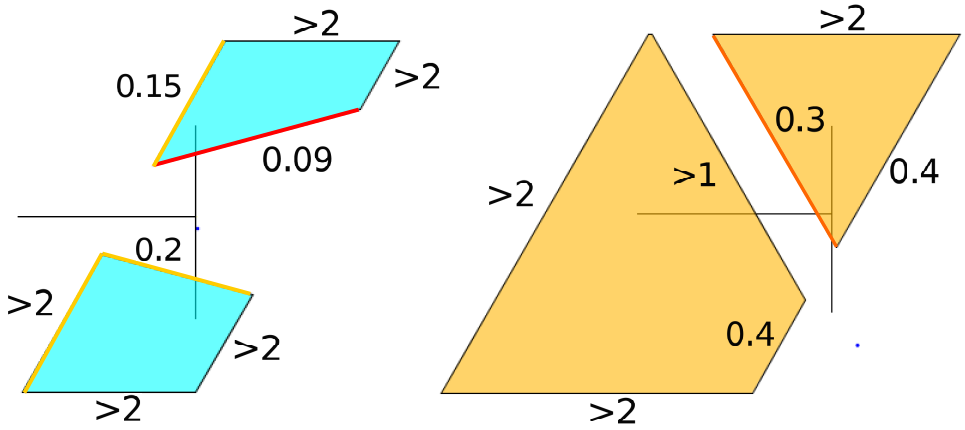

Figure 6.3: Calculation Records

7.4 Geometry and Topology Calculations

The functions associated to the Geometry Calculations 1 and 2 have remained non-negative after extensive experimentation with both the hill-climbing algorithm and the annealing algorithm. The function for the Geometry Calculation 3' exhibits some negative values when I run the annealing algorithm. This happens rather quickly for the reduced capacity, and rarely for the ordinary capacity.

Curiously, I have left the hill-climbing algorithm on overnight for Calculation 3' and it did not turn up a negative value. Neither did a random sample I made with 1 billion points. I think that Calculation 3' barely fails, and that it has some small shallow basins of attraction with negative values in their pits. Just a few applications of the hill climbing would not find these shallow basins, and neither would my random sampling. The annealing algorithm combines random sampling with some exploration of the nearby basins of attraction and thereby does better. All this makes me wonder whether Calculations 1 and 2 would fail under the attack of a better numerical optimization scheme. This is why I say that they probably work but I would not bet my life on it.

The auxiliary calculations for the Topology Lemma, the involving cyclic tensegrities of complexity 4, seem true by wide margins. When I ran 10 minutes worth of the hill-climbing algorithm on the function for Topology Calculation 1 for 10 minutes, the program reached a capacity of $2\sqrt{3} + .23$. When I ran 10 minutes worth of the hill-climbing algorithm on the function for Topology Calculation 2 , the program reached a capacity of $2\sqrt{3}+.94$. The annealing algorithm produces similar results for the Topology Calculation 1, and gets the minimum down to $2\sqrt{3} + .8$ after 10 minutes.

8 References

[**AHLM**] A. Malaga, S. Lelievre, E. Harriss, P. Arnoux, *ICERM website*: https://im.icerm.brown.edu/portfolio/paper-flat-tori/ (2019)

[**CB**], R. Connolly, A Back, *Mathematics and Tensegrity*, in **American Scientist**, Vol 82 **2**, (March-April 1998) pp 142-151.

[**CF**] Y. Chen and E. Fried, *Mobius bands, unstretchable material sheets and developable surfaces*, Proceedings of the Royal Society A, (2016)

[**CKS**] J. Cantarella, R. Kusner, J. Sullivan, *On the minimum ropelength of knots and links*, Invent. Math. **150** (2) pp 257-286 (2003)

[**FT**], D. Fuchs, S. Tabachnikov, *Mathematical Omnibus: Thirty Lectures on Classic Mathematics*, AMS 2007

[**GS**] G. Schwarz, *A pretender to the title "canonical Moebius strip"*, Pacific J. of Math., **143** (1) pp. 195-200, (1990)

[**HF**, D.F. Hinz, E. Fried, *Translation of Michael Sadowsky's paper 'An elementary proof for the existence of a developable MÖBIUS band and the attribution of the geometric problem to a variational problem'*. J. Elast. 119, 3–6 (2015)

[**HW**], B. Halpern and C. Weaver, *Inverting a cylinder through isometric immersions and embeddings*, Trans. Am. Math. Soc **230**, pp 41.70 (1977)

[**MK**] L. Mahadevan and J. B. Keller, *The shape of a Mobius band*, Proceedings of the Royal Society A (1993)

[**Sa**], M. Sadowski, *Ein elementarer Beweis für die Existenz eines abwickelbaren MÖBIUSschen Bandes und die Zurückführung des geometrischen Problems auf einVariationsproblem*. Sitzungsberichte der Preussischen Akad. der Wissenschaften, physikalisch-mathematische Klasse 22, 412–415.2 (1930)

[**S1**] R. E. Schwartz, *The* 5 *Electron Case of Thomson's Problem*, Journal of Experimental Math, 2013.

[**S2**] R. E. Schwartz, *An improved bound on the optimal paper Moebius band*, preprint, 2020

[**W**] S. Wolfram, *The Mathematica Book, 4th Edition*, Wolfram Media and Cambridge University Press (1999).